Article

Influence of Biosynthesized Nanoparticles Addition and Fibre Content on the Mechanical and Moisture Absorption Behaviour of Natural Fibre Composite

Natrayan Lakshmaiya [1] , Velmurugan Ganesan [2] , Prabhu Paramasivam [3] and Seshathiri Dhanasekaran [4,*]

1 Department of Mechanical Engineering, Saveetha School of Engineering, SIMATS, Chennai 602105, Tamilnadu, India
2 Institute of Agricultural Engineering, Saveetha School of Engineering, SIMATS, Chennai 602105, Tamilnadu, India
3 Department of Mechanical Engineering, College of Engineering and Technology, Mattu University, Mettu 318, Ethiopia
4 Department of Computer Science, UiT The Arctic University of Norway, 9037 Tromsø, Norway
* Correspondence: seshathiri.dhanasekaran@uit.no

Abstract: This study looks at how incorporating nanofiller into sisal/flax-fibre-reinforced epoxy-based hybrid composites affects their mechanical and water absorption properties. The green Al_2O_3 NPs are generated from neem leaves in a proportion of leaf extract to an acceptable aluminium nitrate combination. Both natural fibres were treated with different proportions of NaOH to eliminate moisture absorption. The following parameters were chosen as essential to achieving the objectives mentioned above: (i) 0, 5, 10, and 15% natural fibre concentrations; (ii) 0, 2, 4, and 6% aluminium powder concentrations; and (iii) 0, 1, 3, and 5% NaOH concentrations. Compression moulding was used to create the hybrid nanocomposites and ASTM standards were used for mechanical testing such as tension, bending, and impact. The findings reveal that combining sisal/flax fibre composites with nanofiller improved the mechanical features of the nanocomposite. The sisal and flax fibre hybridised successfully, with 10% fibres and 4% aluminium filler. The water absorption of the hybrids rose as the fibre weight % increased, and during the next 60 h, all of the specimens achieved equilibrium. The failed samples were examined using scanning electron Microscopic (SEM) images better to understand the composite's failure in the mechanical experimentations. Al_2O_3 NPs were confirmed through XRD, UV spectroscope and HPLC analysis. According to the HPLC results, the leaf's overall concentrations of flavonoids (gallocatechin, carnosic acid, and camellia) are determined to be 0.250 mg/g, 0.264 mg/g, and 0.552 mg/g, respectively. The catechin concentration is higher than the phenolic and caffeic acid levels, which could have resulted in a faster rate of reduction among many of the varying configurations, 4 wt.% nano Al_2O_3 particle, 10 wt.% flax and sisal fibres, as well as 4 h of NaOH with a 5 wt.% concentration, producing the maximum mechanical properties (59.94 MPa tension, 149.52 Mpa bending, and 37.9 KJ/m^2 impact resistance). According to the results, it can be concluded that botanical nutrients may be used effectively in the manufacturing of nanomaterials, which might be used in various therapeutic and nanoscale applications.

Keywords: nanocomposites; natural fibre; biosynthesis; neem leaf; aluminium oxide; sisal fibre; flax fibre

1. Introduction

The rise of the fibre-reinforced composites business in the automobile industry has triggered a search for environmentally friendly natural resources. Due to their numerous benefits to engineering construction, composite materials have been widely employed in transportation applications for decades, replacing traditional metals [1]. The lower-weight features of composite materials are particularly intriguing in transportation applications

since they may reduce energy consumption. Composite materials, in addition to being lighter than steel, provide several other advantages [2]. Steel has lower fatigue resistance than composite materials. This feature has made composite material utilization in structural applications more appealing. Despite their various benefits, composites are primarily made of artificial fibres such as graphite, glass, and fibreglass.

This situation negatively influences climate change since synthetic fibres are not recyclable. Lignocellulose fibres are being employed to substitute artificial fibres in composite goods, perhaps making them more ecologically friendly. Natural fibres may be better for the environment than synthetic materials [3]. Natural textiles also provide several advantages over synthetic fabrics, including superior characteristics, low cost, low density, lower power consumption, and are ecologically friendly, non-abrasive, non-toxic, and long-lasting [4]. The significant advancement in the mechanical features of sisal-based polymer matrix composites was considered remarkable amongst the numerous natural fibre mixtures. Sisal fibre, derived from the Agave sisalana tree, is one of the most frequently used natural materials and can be quickly grown in any region of Earth. It comes from the sisal plant. According to the global context, the rate of sisal fibre production is expanding due to its wide range of uses [5].

Hybrid composites comprise more than two fibres in a unified framework. By addressing distinct mixtures' defects, hybridization can improve the mechanical properties of biological-fibre-reinforced polymers [6]. Flaxseed (*Linum usitatissimum* L.) represents the only intensive agriculturally significant plant in the Linaceae category, including four groups with 400 varieties. Flaxseed, the very first textile formed from grains and solidified into such matrices, was grown from around 5000 B.C. and also unearthed in Egyptian tombs. It is one of the most commonly used bio-fibres [7,8]. Flax has been a critical crop for decades due to its uses in filaments and petroleum. Flaxseed has undergone extensive research and development for favourable features such as herbicide resistance, biogenic drought tolerance, higher oil content, and cellulose qualities. Flaxseed is a perennial tree, having 16–32 mm branches that develop to 0.5–1.25 m in height [9]. In flaxseed cultivation, natural plants are much more effective in low sites, where ambient abiotic stresses induce considerably more morbidity than in rich soils [10].

Moreover, it has been shown that lignocellulosic fibre-based composites exhibit little nick compassion compared to artificial composites. Organic filament-strengthened composites have some benefits over synthetic fibre composites but also have certain disadvantages. The hydrophilic characteristic of cellulosic fibres makes them incompatible with polymeric matrixes, which is one of their primary weaknesses [11]. Because of their hydrophilicity, lignocellulosic materials absorb many environmental moistures. On the other hand, chemical approaches can improve the fibre-polymer matrix interaction. Natural materials are often pre-treated before being used in composites to improve their interactions and produce high mechanical strength. The surface properties of the filaments are altered during treatment, resulting in a heavily cross-linked interfacial region with covalent bonding connections between the reinforcement and the matrix. Alkali pre-processing is one of the most used pre-treatment methods for changing the surface morphology of fibres and dissolving high lignin content, waxes, and impurities [12,13]. During the alkaline chemical modification, the hydroxyl groups of lignocellulosic materials are ionized particles with an alkoxide. The hydrophilic character of the filaments is concentrated and the reinforcement–resin interaction is improved. Furthermore, chemically processed organic filaments have been demonstrated to exhibit improved fibre-dispersal capabilities, resulting in increased stress transmission across the fibre–matrix interaction due to the reduced quantity of hydrophilic groups in the fibres [14].

In the current world of materials and industrial engineering, nanoparticle-reinforced polymers are one of the most reliable and well-known composites for constructing models [15,16]. When nanocrystals are used for reinforcing, several investigations have shown that the synthetic behavioural properties improve more than the mechanical characteristics. Aluminium oxide is another essential ingredient employed for reinforcements due to its

exceptional electromagnetic, structural, and thermodynamic characteristics. It has the breadth of a single organism and a multi-dimensional hexagonal strategy. It has been used in many electronic and optical devices [17]. Due to its endurance, it has now been proven to be an excellent filler in epoxy restoration materials. The existence of an oxide position in nano-aluminium material, which acts as a strong adhesive throughout the matrix, is also the leading cause [18].

Implementing green techniques to produce nanoparticles is becoming an active issue in nanotechnology. Because of its numerous uses in physics, economics, physiology, and healthcare, work on synthetic nanoparticles and their characterization has been a developing subject of nanotechnology for the last twenty years [19]. Natural nanoparticle manufacturing techniques based on microbes, enzymes, fungi, and flowers derived from plants were proposed as ecologically sound replacements for chemical and physical approaches. Manufacturing nanoparticles using plants or plant components might sometimes be beneficial over other biological methods because it eliminates the complex procedures of sustaining bacterial culture [20]. Since Al_2O_3 NPs were chemically bio-inert and hydrogel was more durable, they have received exceptional interest in the leading edge of specialized development in the synthesis and development of contemporary antibacterial drugs with sustainable biological properties. Many researchers have already addressed the bioavailability of Al_2O_3 NPs ceramics. Highly pure Al_2O_3 NPs are also the first Phyto commonly used in clinical applications and it was suggested that the life of Al_2O_3 NPs is greater than that of the people affected [21,22]. As a result, Al_2O_3 NPs could be used in various fields, including structural ceramics catalysis, textiles, wastewater, and protein isolation. Furthermore, Al_2O_3 NPs have many biological uses, including biosensing, Phyto, and therapeutic agents [23].

Because of its eco-friendly character and non-harmful approach, green systemization hugely influences today's and tomorrow's societies. Plant leaves were formerly used to make nanopowders such as SiO_2, TiO_2, and Al_2O_3. The aluminium oxide (Al_2O_3) nanofiller utilized in the method is extracted from the 'Neem Leaf' using a specific ratio of aluminium nitrate. The main objective of the investigation is to find the effectiveness of fibre and nanoparticle weight % in the mechanical and moisture absorption behaviour of sisal/flax-based hybrid composites. The compression moulding technique was used to fabricate the hybrid composites. After fabrication, the composites were tested for various mechanical properties such as tensile, flexural, and impact.

2. Investigational Works

2.1. Reinforcement Materials

The natural fibres sisal and flax were used in this investigation. Rithu Natural Fibres Industry in Salem, Tamil Nadu, India, supplied both fibres. The matrix components used in this investigation were Chembion A-type epoxy resin with a density of 1.12 to 1.14 g/cm^3 and aliphatic amine B-type hardener with a density of 1.02 g/cm^3. Naga Chemical Industry supplied resin and hardeners in Chennai, Tamil Nadu, India. The family of fundamental components, or cured final product, of elastomers is known as epoxy. Epoxy resins are epoxide-containing reacting prepolymers and polymers, commonly known as polyepoxides. Epoxy functional groups are also known as epoxy structural features. The supplier suggested that the mixing ratio of epoxy resin and hardener be 3:1. Furthermore, the viscosity of the epoxy resin was 550 MPa/s, the pot life was 30 min, and the hardening time was 24–36 h at room temperature. Figure 1 shows the photographic images of fibres and chemicals used in the present research.

Figure 1. Photographic Images of (**a**) sisal fibre; (**b**) flax fibre; (**c**) Epoxy matrix; and (**d**) NaOH pallets.

2.2. Alkaline Treatment

One of the most common treatments for natural fibres used in composite materials is the alkaline treatment. In this study, sisal and flax fibres were submerged in varying concentrations of NaOH (0, 1, 3, and 5 wt.%) solution for 4 h. New sisal and flax fibres were gathered and carefully cleaned for alkalization. The fibres were then rinsed multi times with distilled water to eradicate any remaining chemicals. The mercerization reactions on reinforcement are expressed in Equation (1) [11].

$$\text{Fibre} - \text{OH} + \text{NaOH} \rightarrow \text{Fibre} - \text{O} - \text{Na} + \text{H}_2\text{O} \tag{1}$$
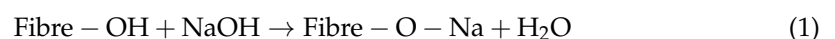
2.3. Preparation of Aluminium Oxide Nanopowder

Distilled water was often used to clean neem leaves. Neem leaves were chopped into small pieces and combined with 350 mL of distilled water before being cooked for 30 min on a heating mantle at 70 °C and then chilled. Filtration was carried out at 1200 rpm, 15 °C, and for 40 min. The reductions of the metal ions through leaf extract led to the formation of synthesized nanoparticles that are quite stable in solutions. The colour change occurred when we added aluminium nitrate chemical agents to the leaf extract. This colour change indicated the formation of nanoparticles in each stage. In the method, leaf extract containing aluminium nitrate was employed. Aluminium nitrate was combined with distilled water in a 4-molar solution. The leaf extract in the beaker was mixed with aluminium nitrate in the separator funnel at a 4:1 ratio using a magnetic stirrer at 800 rpm. The original green tint changed to a white-coloured residue after 40 min, indicating the presence of aluminium oxide nanopowder. The block diagram of Al_2O_3 NPs preparation can be seen in Figure 2. Following the production of a white residue, spinning at 15,000 rpm, 20 °C, and for 40 min, it was combined with the fractional distillation. These techniques were performed four times in a row to maximize nano powder separation. In the last stage, nano powder was

baked in an oven for 5 h at 150 degrees Celsius. The chemical reactions of Al_2O_3 NPs formations are expressed in the following Equations (2) to (4).
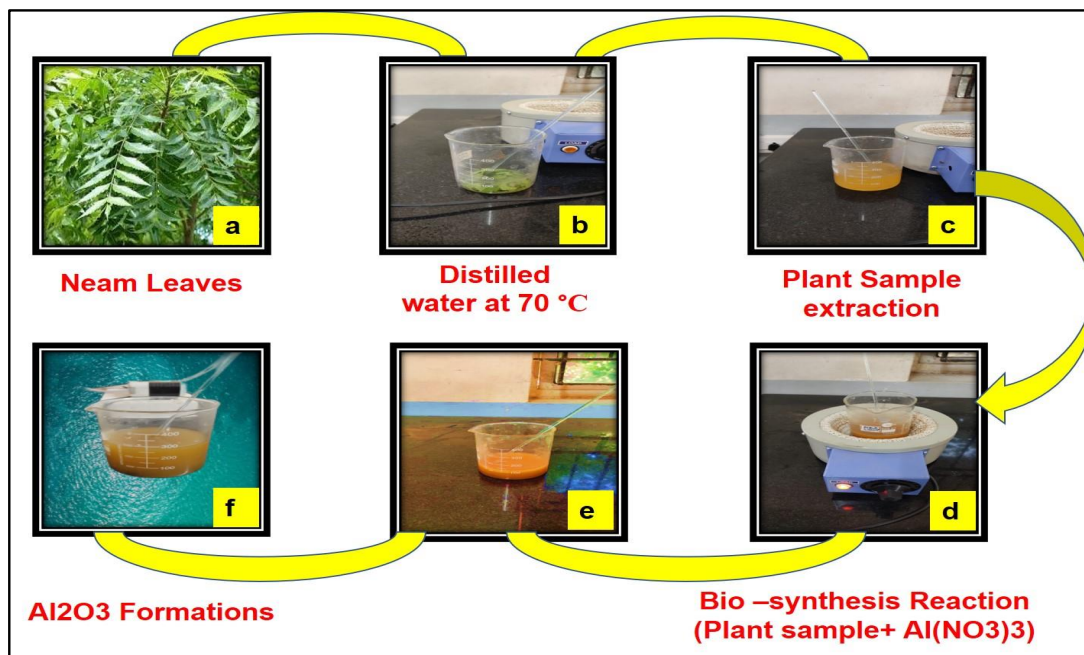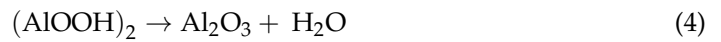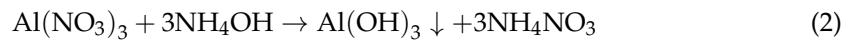
$$Al(NO_3)_3 + 3NH_4OH \rightarrow Al(OH)_3 \downarrow + 3NH_4NO_3 \tag{2}$$

$$Al(OH)_3 \rightarrow AlOOH \downarrow + H_2O \tag{3}$$

$$(AlOOH)_2 \rightarrow Al_2O_3 + H_2O \tag{4}$$

Figure 2. Demonstrates the Al_2O_3 NPs preparations through biosynthesis process (**a**) Heating the neem leaf; (**b**) Formation of leaf extract after centrifugal process; (**c**) Mixing leaf extract with $Al(NO_3)_3$ solutions; (**d–f**) Colour Modification subsequent to fraternization.

2.4. Hybrid Composite Preparations

The sixteen composite samples were fabricated as per the Taguchi L16 orthogonal array design. The composite was made with sisal/flax fibres and nano aluminium utilising compression moulding. A stainless steel mould measuring $150 \times 150 \times 3$ mm was used to fabricate the hybrid composites. Mechanical stirring with a glass rod at 150 RPM dispersed varied quantities of nanoparticles (0, 2, 4, and 6 wt.%) in the epoxy resin. The matrix mixture was evenly distributed throughout the fibre layers of the mould. The mould was connected and placed in the compression moulding at 50 bar pressure and 120 °C. The desiccators prevented any additional moisture absorption by the hybrid composite material. Table 1 lists the constraints and their levels utilized for the present research. Table 2 shows the L_{16} Taguchi orthogonal array.

Table 1. Constraints and their stages for hybrid composite.

Sl.No	Constraints	Stages			
		S1	S2	S3	S4
1	Sisal Fibre (wt.%)	0	5	10	15
2	Flax Fibre (wt.%)	0	5	10	15
3	Nano Al_2O_3 Filler (wt.%)	0	2	4	6
4	NaOH concentration (wt.%)	0	1	3	5

Table 2. L_{16} Taguchi Orthogonal Array.

Sl.No	Sisal Fibre (wt.%)	Flax Fibre (wt.%)	Nano Filler (wt.%)	NaOH (wt.%)
1	0	0	0	0
2	0	5	2	1
3	0	10	4	3
4	0	15	6	5
5	5	0	2	3
6	5	5	0	5
7	5	10	6	0
8	5	15	4	1
9	10	0	4	5
10	10	5	6	3
11	10	10	0	1
12	10	15	2	0
13	15	0	6	1
14	15	5	4	0
15	15	10	2	5
16	15	15	0	3

2.5. Characterization of Hybrid Composites

All of the hybridized nanocomposites were mechanically characterized initially. The Instron 1195 type Universal Testing Machine (UTM) with load limits of 5 KN and a crosshead speed of 2 m/min was used to examine flexural and tensile properties. For the tension experiment, the laminated hybrid samples were cut and converted to ASTM D 638-03 replicas with measurements of $150 \times 15 \times 3$ mm, ASTM D-790 (width 10 mm, length 125 mm, and thickness 3 mm) for bending behaviour. The sample was placed inside the tensometer's attachment. The equipment was turned on as the tensometer's stepper motor progressively transmitted the tensile force to the sample. The deformation value was assessed using the strain gauge linked to the tensometer. After applying a critical load to the specimens, they were sliced into two pieces. If the specimen was flexural, it was sliced into three sections. The computer linked to the tensometer recorded the stress and strain values. The un-notched Izod impact test was performed on the composite sample using Tinius Olsen (Model Impact 104, 9.81 kN pendulum capacity) pendulum impact testing equipment with dimensions of $64.3 \times 12.7 \times 3$ mm at room temperature by ASTM D 256. SEM (A Zeiss SUPRA 55-VP, 12 KV model with 10, 20 and 200 μm magnification) was employed to examine broken hybrid materials at a microscopic (fractographic) level. Before SEM clarity, the specimens were laved, dehydrated, and surface coated with 10 nm of gold to increase the electrical conductivity of the composites. All of the mechanical testing and microstructural analysis were carried out in the materials testing laboratory at Sathiyabama University, India.

2.6. Water Absorption Behaviour

Water absorption experiments were performed by UNEEN ISO 62:2008 to investigate the water uptake behaviour of natural-fibre-reinforced nano filler-based epoxy composites. Composite samples were submerged in a water bath for an extended period until saturation was achieved.

The samples were dried for 24 h in a 45 °C oven before being cooled to room temperature. The dehydration procedure was repeated until the items' weight remained consistent (weight W_1). Following 60 h, the specimens were removed from the water and measured (weight W_2) with a digital scale immediately after being dried with a dry towel. This procedure was repeated throughout the 60 h of water immersion to weigh the specimens

regularly. The following Equation (4) was used to calculate the water absorption behaviour of composites. Figure 3 shows the photographic images of water absorption behaviour.

$$\text{Water Absorption} = \frac{W_2 - W_1}{W_1} * 100 \tag{5}$$

Figure 3. Photographic image of water absorption behaviour experiment.

2.7. XRD Analysis

A ULVAC-PHI6000 Probe III X-ray diffractometer with Cu-Kα1 emission at 50 kV, 30 Ma, and = 2.41 was employed for X-ray diffraction (XRD). These X-ray diffraction patterns were examined at an ambient temperature of 10 to 80° (2Θ) at a rate of 0.05 min^{-1}. The diffraction peaks of biosynthesized nano Al_2O_3 NPs were compared to the JCPDS database. Furthermore, the morphology of the powder was examined using a 150-CX transmission electron microscope (TEM) at 100 kV.

2.8. HPLC (High-Performance Liquid Chromatography) Analysis

The polyphenols in Azadirachta indica aqueous extracts were quantified using an Agilent 1100 Model HPLC system with diode array detection and injector valves with a 20-µL measured flow. Substances were segregated on a 4.7 mm 260 mm, i.e., 5 m pore diameter, Phenomenex SB RP-C20 column guarded by only a guarding column filled with the same packaging. HPLC-grade methanol (Part A) and water were used as the sample solvent system (Part B). Its flow rate was constantly maintained at 1.0 mL/min [24]. The injection volume was maintained at 10 µL.

3. Result and Discussion

3.1. Characterizations of Al_2O_3 Nanoparticles

The current study concerns the immediate functionalization of Al_2O_3-NPs utilizing raw neem leaves. A yellowish-brown white precipitate was observed when a neem leaf extract and an aqueous phase of aluminium nitrates were microwave-irradiated for 6–10 min. Before even being employed by the characteristics and microbiological contact experiments, Al_2O_3-NPs were characterized using XRD, SEM, and TEM investigations to confirm the main and secondary sizes and forms. In Figure 4a, the SEM micrographs of Al_2O_3-NPs showed approximately spherical shell NPs with maybe some aggregation [25,26].

The XRD characteristic of Al_2O_3-NPs exhibited three diffraction patterns (115, 119, and 215) is shown in Figure 5 with spikes around it (115 and 119 being among the strongest). Powder X software was used to identify these peaks, which were discovered to correlate with the composition of Al_2O_3 (JCPDS card No. 42-1468). The form of Al_2O_3 nanoparticles

were investigated using imaging from a transmission electron microscope (TEM). These specimens were randomly scanned using a 150-CX TEM at 100 kV. Based on the observed data the calculated nanoparticle size is 38.61 nm, which is related to the most intensive crystalline sector (115) [27]. Most nanomaterial shapes were spheres and triglycerides in the 10–500 nm region, as indicated by the TEM image (Figure 4b). Following the figure, the majority of nanomaterial appeared spherical. The XRD image confirmed it as well. The sharpened characteristic of the XRD analysis reveals the crystalline phase of the prepared NPs. There are no further diffraction patterns from Al_2O_3 NPs in the XRD pattern, demonstrating the excellent phase purity of the synthesized material [28].
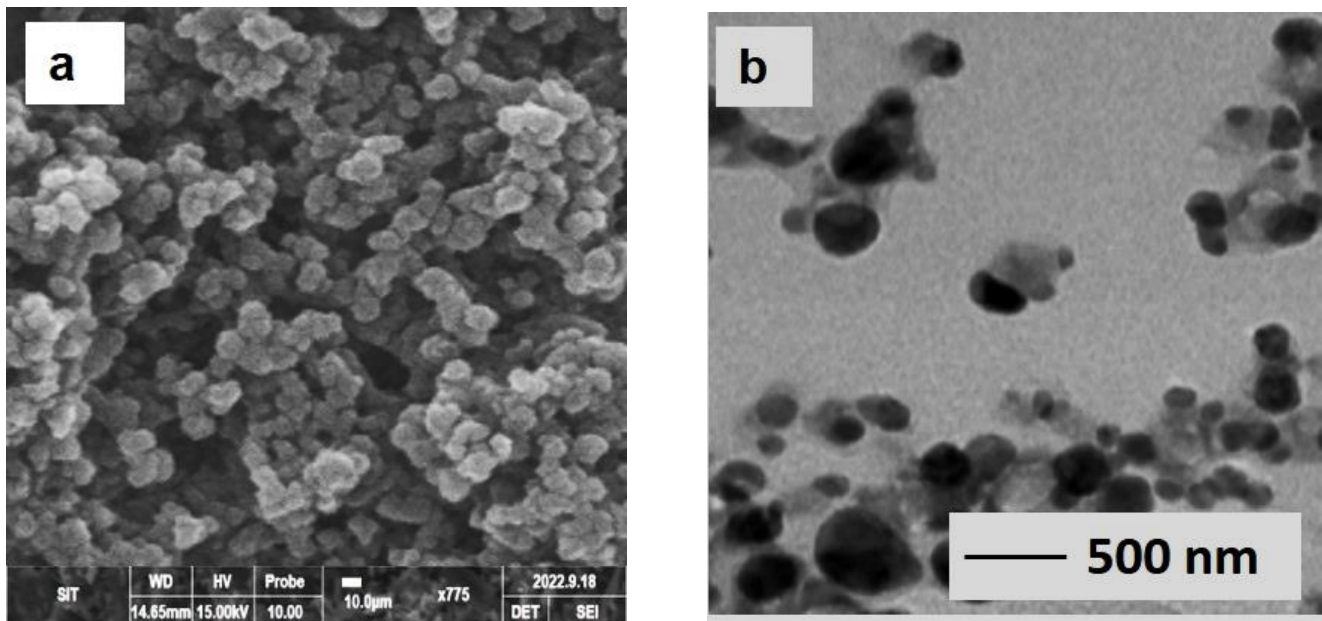
Figure 4. Microstructural analysis of (**a**) SEM images of Al_2O_3 NPs; (**b**) TEM Images of spherical structured nanoparticles.
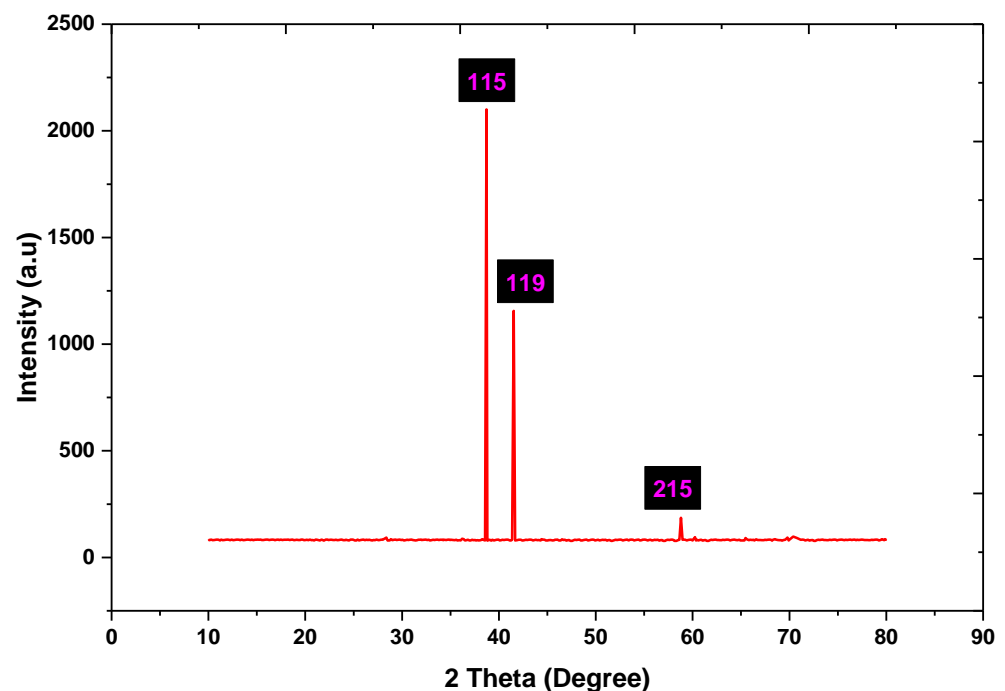
Figure 5. XRD patterns of Al_2O_3 nanoparticles.

The aqueous extracts of neem leaves appeared lighter yellow in hue, whereas the aluminium nitrate solutions appeared white. Initially, the light-yellow hue was generated by adding neem leaf extracts to an aluminium nitrate solution. The mixture was modified and turned light green following a half-hour of heating at 70 °C with mixing, demonstrating the creation of Al_2O_3 NPs. The hue of aluminium oxide nanoparticles ranges from yellow to light green, according to the size and structure of the Al nanoparticle [29]. The light-green hue was created due to the conversion of Al (III) to Al (0) and the significant improvement in the internal and subcutaneous production of Al NPs. The ultraviolet spectroscopy of biologically-synthesized Al_2O_3 NPs by neem leaves revealed intense peaks at 543 nm. The wide peak indicates (Figure 6) the presence of large-sized nanoparticles. The MIE concept was employed to analyse the spherical shape and tiny size of NPs formed in the reaction medium, which was identified by producing a single surface plasmon band for Al_2O_3 NPs [30].
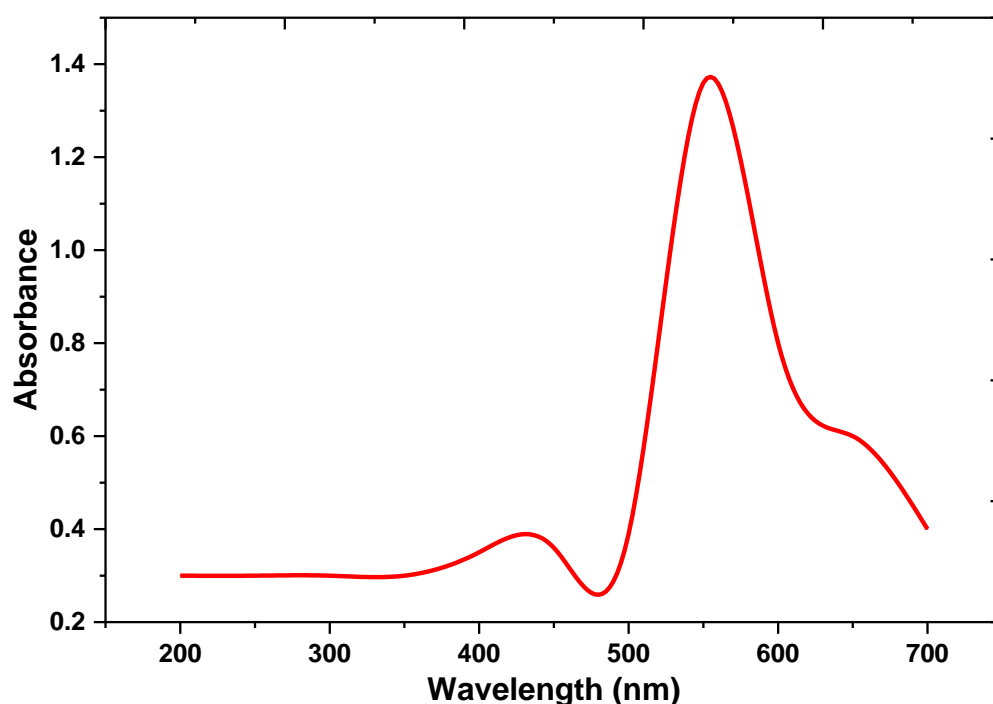

Figure 6. Ultraviolet spectroscopy patterns of Al_2O_3 nanoparticles.

3.2. HPLC (High-Performance Liquid Chromatography) Analysis

A technique is being developed to determine the concentration of polyphenols. Several studies have been described to quantify chosen polyphenols in terms of their biological and medicinal importance. As previously noted in the reference section, the emphasis is placed on significant antioxidants. Zhang et al. [31] adjusted HPLC parameters for simultaneously estimating 14 phenolics in grapes, including gallic acid, caffeic acid, and catechin, because they have significant biochemical effects. Additional research estimating polyphenols such as gallic acid, catechin, and caffeine in tea extracts has been published [32,33].

An earlier study has shown that catechin may serve as a reductant and cap Al_2O_3 NPs through green packaging. As a result, we experimented with altering the volumetric content of a solvent system (50:50 acetonitrile: water) with fluid velocity. A solitary maximum absorbance was produced with 50:50 and was conducted for greater study in contrast to specific other proportions that produced many signals, which may be related to strongly adsorbed elements inside the solvent system or detector responses. Nevertheless, it may be tweaked or tested using HPLC preservation performance measures such as specimen solvents, heating rates, and solvent system constituents. The established process was performed three times for additional study [34]. Chromatograms have been obtained for gallic

acid, caffeic acid, and catechin values at 20, 30, and 40 mg/L. The specimen (a neem leaf extraction) was then injected and analysed. Figure 7 shows the chromatograms for 20 mg/L. The presence of numerous peaks could be attributed to impurity influences. Calculated values of gallic acid, caffeic acid, and flavonoid sample solutions were shown at 20, 30, and 40 mg/L. A chromatogram for the specimen is shown in Figure 7. The leaf extract specimen included organic material containing phenyl rings, including phenolic acids. Among them were aromatic ethanol, o-guaiacol, 2,3-dihydrobenzofuran, p-vinilguaiacol, and dimethyl phthalates. Polyphenol chemicals reduce reagents for nanoparticles, enveloping particles and giving them exceptional resilience to prevent aggregation [35]. According to the findings, the leaf's overall concentrations of flavonoids (gallocatechin, carnosic acid, and camellia) were determined to be 0.250 mg/g, 0.264 mg/g, and 0.552 mg/g, respectively. The catechin concentration is higher than the phenolic and caffeic acid levels, which could have resulted in a faster rate of reduction. This contributes to the formation of Al_2O_3 NPs [36].
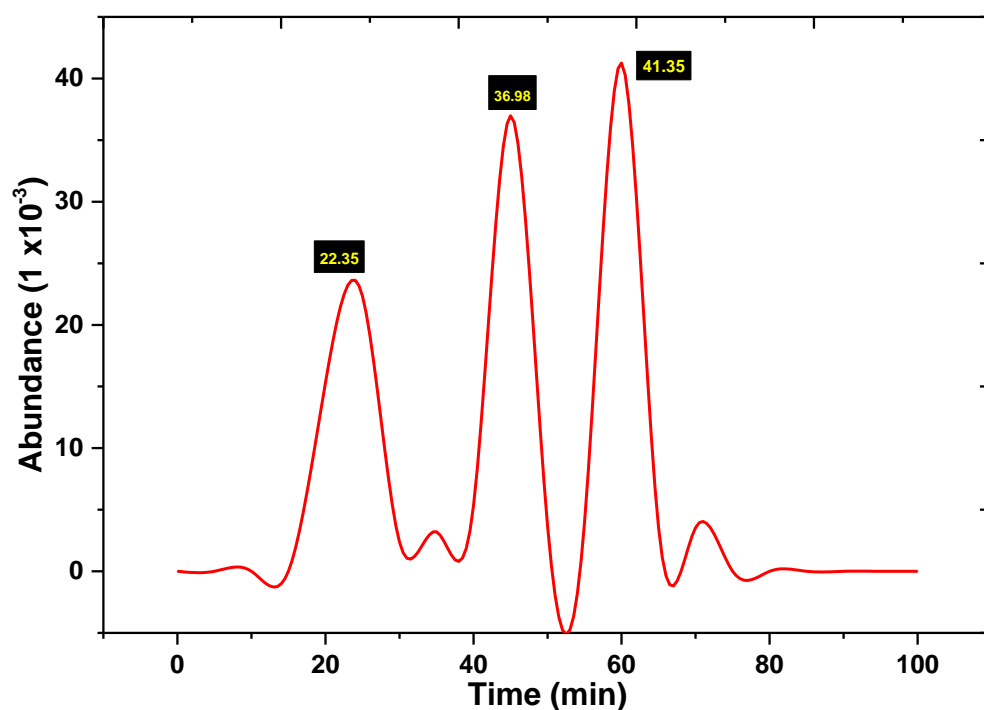

Figure 7. Chromatogram of the samples of neem leaves extract.

3.3. Mechanical Properties

3.3.1. Consequence of Fibre Content

The average tension, bending, and impact behaviours of the sisal/flax-based hybrid nanocomposite with 0, 5, 10, and 15% fibre content are shown in Figure 8a,b. The mechanical characteristics of hybrid composites improve with increasing fibre loading up to 10% but then decline to 15%. When compared to a pure epoxy composite, adding 5% sisal or flax to the epoxy composite increases its strength. The 5 wt.% fibre-based composites showed lower strength when compared to others. This is because compared to other fibre content, the 5 wt.% content composites have poor adhesion to the matrix. Therefore, the stress transfer rate is low in 5 wt.% fibre composites. Consequently, matrix-high regions occurred in the composites through a deprived fibre-content link [37]. The fibre reinforcement was pulled out of the matrices when overloaded in this state. It demonstrates that the sisal/flax reinforcing effect of 5% in the epoxy is inadequate to tolerate the applied stress. The material's overall performance rises as the sisal/flax content increases from 5% to 10%. At 10% fibre-reinforced composite, extreme ductile strength is 59.94 MPa, bending is 149.52 MPa, and impact is 37.0 KJ/m^2. This is primarily due to the formation of good

bonding between the fibres and the matrix, which occurred due to the natural-fibre pretreatment (NaOH Treatment). It reduced the void content in the composite by presenting the additional short fibres and confirming adequate load distribution throughout the layers. Figure 9 shows the mean value of the tensile strength of various input parameters.
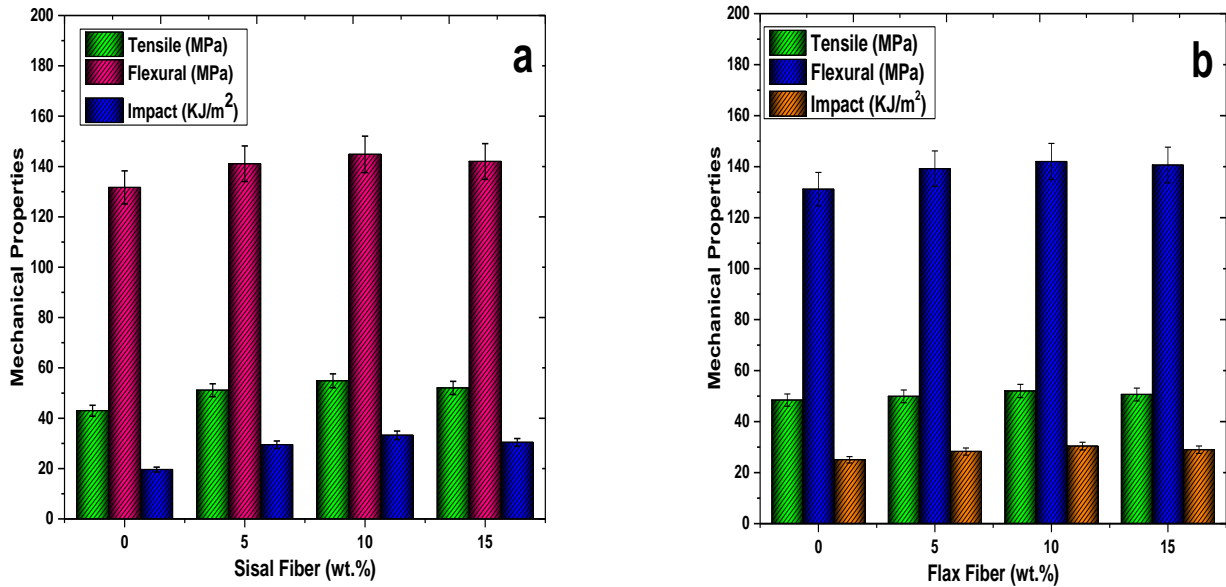

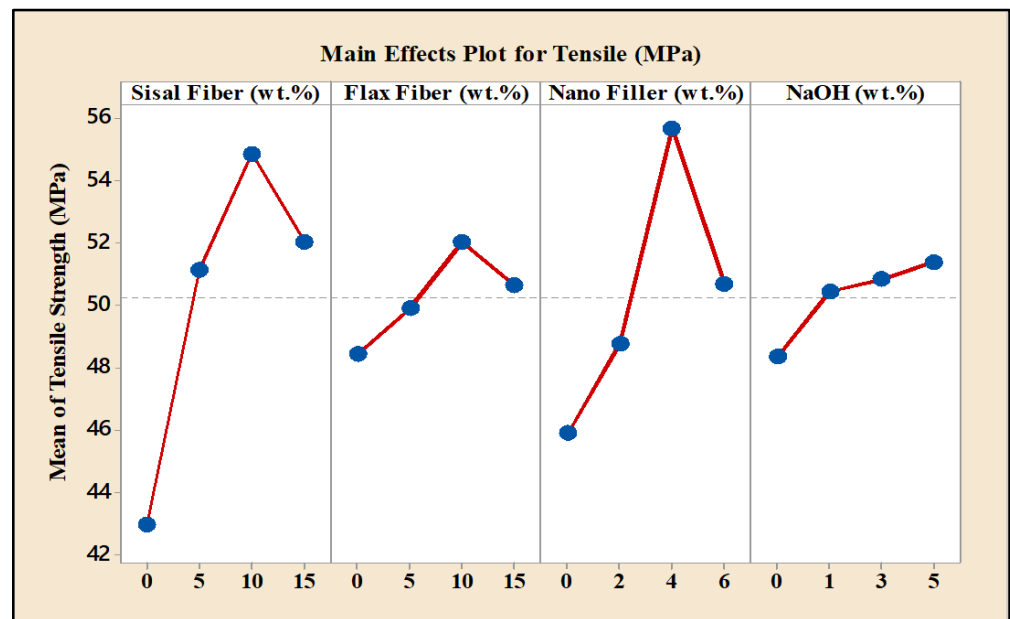**Figure 8.** Average value of Mechanical Properties (**a**) wt.% of Sisal Fibre; (**b**) wt.% of Flax Fibre.

Figure 9. Mean Values of Tensile Behaviour of Hybrid Composites with various input parameters.

When 15 wt.% fibre loading was used, the mechanical strength of the composite was reduced. The cause of this might be that the matrix volume % is insufficient to ensure excellent bonding, resulting in poor wettability between the fibres and the matrix and the formation of a fracture in the matrix. It is clear from the data that the 10 wt.% fibre-loaded composite has better mechanical characteristics than the other combinations. The most likely cause is that as fibre content increases, the applied stress is adequately communicated to the fibres via the matrix. It contributes to the ability to bear tensile solid, flexural, and impact loads. The fibre concentration of 10% is better for optimum load distribution in the composites.

3.3.2. Consequence of Nano Filler Loading

The composition of the fillers, polymer, polymer filler adherence, cross-linking chemicals, and preparation techniques influence the mechanical characteristics of a composite. As a result, any enhancement in the characteristic is assessed in comparison to a polymer matrix that has experienced the same procedure. The fillers are saturated at room temperature by the polymer solution, which is then hardened using a cross-linking agent. Tensile, flexural, and impact properties typically improve as the nano filler loading in the formulation increases. Figure 10 demonstrates the average values of mechanical strength based on nano Al_2O_3 particles. The adherence between the epoxy and the filler reduces beyond a specific limit of filler content based on the treatment methods, leading to a decline in the strength of the end goods [38].
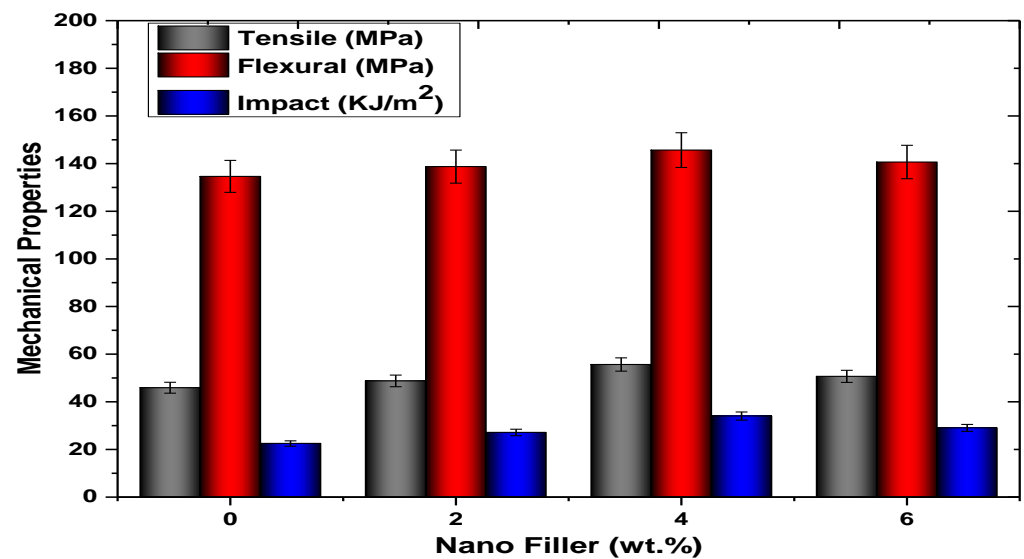

Figure 10. The average values of mechanical strength based on nano Al_2O_3 particles.

The overall tensile strength of the material during the 4 weight percentage of nano Al_2O_3 is 59.94 MPa, the bending is 149.52 MPa, and the impact is 37.0 KJ/m^2. The composite's elasticity decreased somewhat, with a filler loading of 6%. That decrease is attributed to the filler's difficulty sustaining stresses transferred by polymeric composites, as well as poor interfacial interaction resulting in meaningless gaps among fillers and substrate elements, resulting in unsatisfactory outcomes [39]. Whenever the filler loading is excessive, the polymers have a more challenging time entering the tiny diminishing spaces among the fillers, resulting in poor soaking and a decrease in load-transfer effectiveness at the filler–resin contact. The epoxy resin adheres well to various surfaces and may be strengthened further by adding fibres or nanoparticles. Figure 11 Demonstrates the mean values of bending strength based on the different input parameters.

3.3.3. Effect of NaOH Concentration

NaOH processing, also known as mercerization, is a common form of pre-treatment for organic textiles. Due to the apparent alkali treatment, the price of lignocellulosic materials is rising compared to crystal cellulose. The hydroxyl group in the framework was eliminated due to this procedure. In NaOH circumstances, the composite showed a positive outcome in all categories [40]. The mean values of tension, bending, and impact behaviour of sisal/flax-based hybrid composites are shown in Figure 12. Figure 12 shows that the most excellent tensile, flexural, and impact strength values were 59.94 MPa, 149.52 MPa, and 37.9 KJ/m^2 at 5% NaOH. Eliminating impurities from the fibre's surface was not as good at lesser NaOH concentrations (1 and 3 wt.%), resulting in weak fibre binding with matrices. The 5% NaOH pre-treatment with 4 h of alkali increased exterior adhesion by eradicating natural and other foams, resulting in a difficult topography as-

pect of the surface. Sisal and flax fibres were chemically pre-treated with a 5% sodium hydroxide (NaOH) preparation for 4 h to remove hydrophilic hydroxyl collections and impurities from roughage fibres. Even with the matrix material, this will improve fibre interactions and durability [41]. This enhances the mechanical and microstructural characterization through growing polymerisation stages and fibres' crystal structures. Figure 13 shows the mean impact strength values of sisal/flax hybrid composites based on various input parameters.
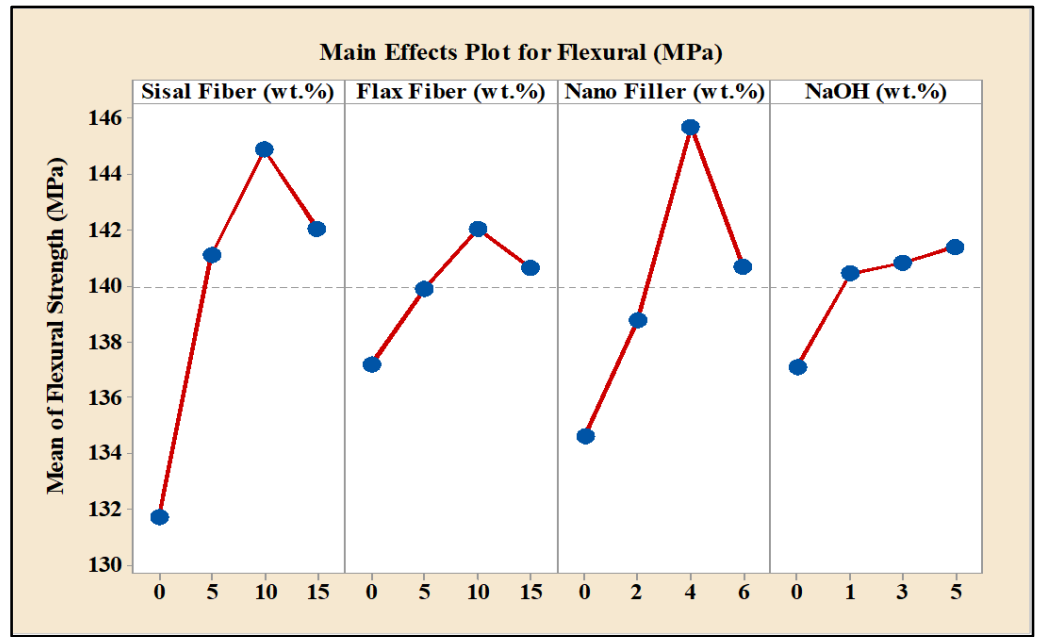
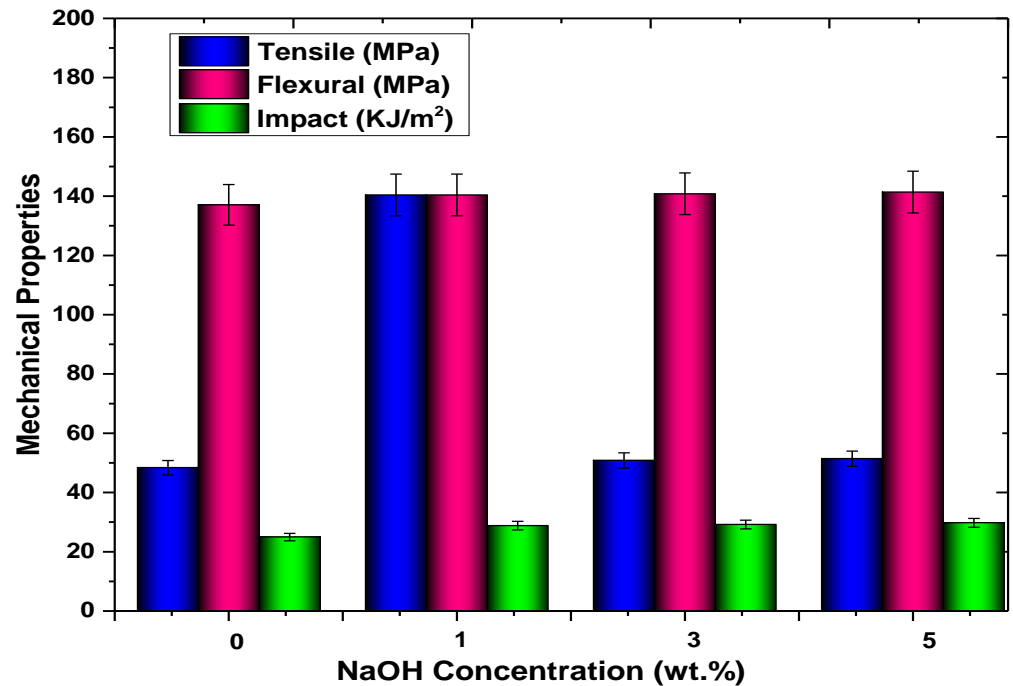**Figure 11.** Mean Values of Bending Behaviour of Hybrid Composites with various input parameters.

Figure 12. The average values of mechanical strength based on NaOH concentrations.
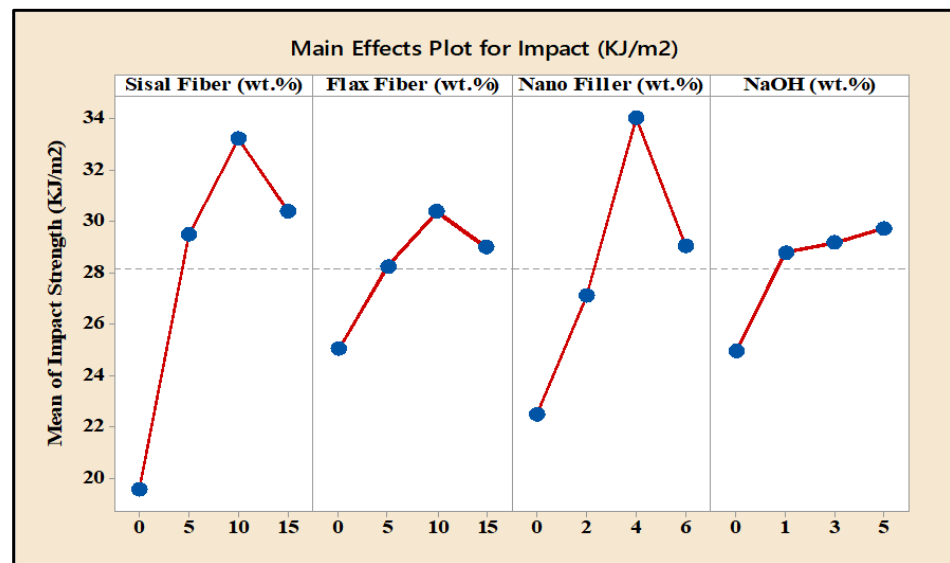
Figure 13. Mean Values of Impact Behaviour of Hybrid Composites with various input parameters.

After NaOH treatment, the fibres were extensively rinsed with fresh and deionized water to eliminate the tiny amounts of NaOH. The XRD scans showed no indication of a greater NaOH concentration in the fibre. Except for peaks at 115, 119, and 215, the remaining peaks demonstrated the NaOH presentation in the fibre mat. Only at greater concentrations (5 wt.%) of NaOH processes is sodium aluminate formed. The content of NaOH in such samples appears to be a factor in the production of sodium aluminate from the residual. This shows that greater NaOH levels combined with extremely high temperatures promote the synthesis of aluminate, the substrate for sodium hydroxide nanoparticles [42]. The XRD data show that the concentration of HCl did not affect the procedure. Previous research has found that the proton content highly influences the leaching rate at the start of the reaction in the anion of the oxide (Cl). Larger HCl levels result in much less acid ionization, which reduces the extraction rate and processing efficiency because a rise in titratable acidity raises the number of metallic ions in the solutions. The formation of sodium aluminate is expressed in Equation (6)

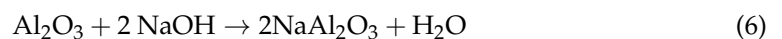$$Al_2O_3 + 2\,NaOH \rightarrow 2NaAl_2O_3 + H_2O \qquad (6)$$

Figure 14a–d show SEM images of plain epoxy, untreated, and various % alkaline-treated fibre-reinforced composites after tensile behaviour, which may be used to measure the degree of adhesive quality between the fibre reinforcement and the polymer matrices. When opposed to alkaline-treated fibres, untreated fibres exhibit more holes and voids. The discrepancy in bonding among organic compounds and the adherence of fibres in a specific location caused these voids to emerge. These spaces are minimised in treated fibres due to the alkaline solution reacting with the fibres, resulting in the creation of acetic cellulose and the insemination of hydroxide deposits, both of which modify the fibres' binding properties [43]. Figure 14a shows the microstructural image of plain epoxy resin. Figure 14b–e show the microstructural images of 0 wt.%, 1 wt.%, 3 wt.%, and 5 wt.% concentrations of NaOH pre-treated fibre-based composites. Figure 14e shows fewer fibre pullouts compared to other images. This may reflect the good bonding between the reinforcements and the matrix. This also helps to enhance the interfacial adhesion among the composite systems. The final result was to increase the mechanical strength of the composites. Figure 14f–h show the microstructural images of 5 wt.% NaOH pre-treated composites under a hybrid composite's tensile, flexural, and impact behaviour. As compared to Figure 14a,b and Figure 8f–h reveal fewer voids and fibre pullouts. They also have evidence of increased bonding strength between the reinforcement and the matrix. The

mentioned microstructural image reveals that the 5 wt.% of NaOH pre-treatment effectively alters the fibre surface. It has helped enhance the hybrid composites' mechanical strength [44].
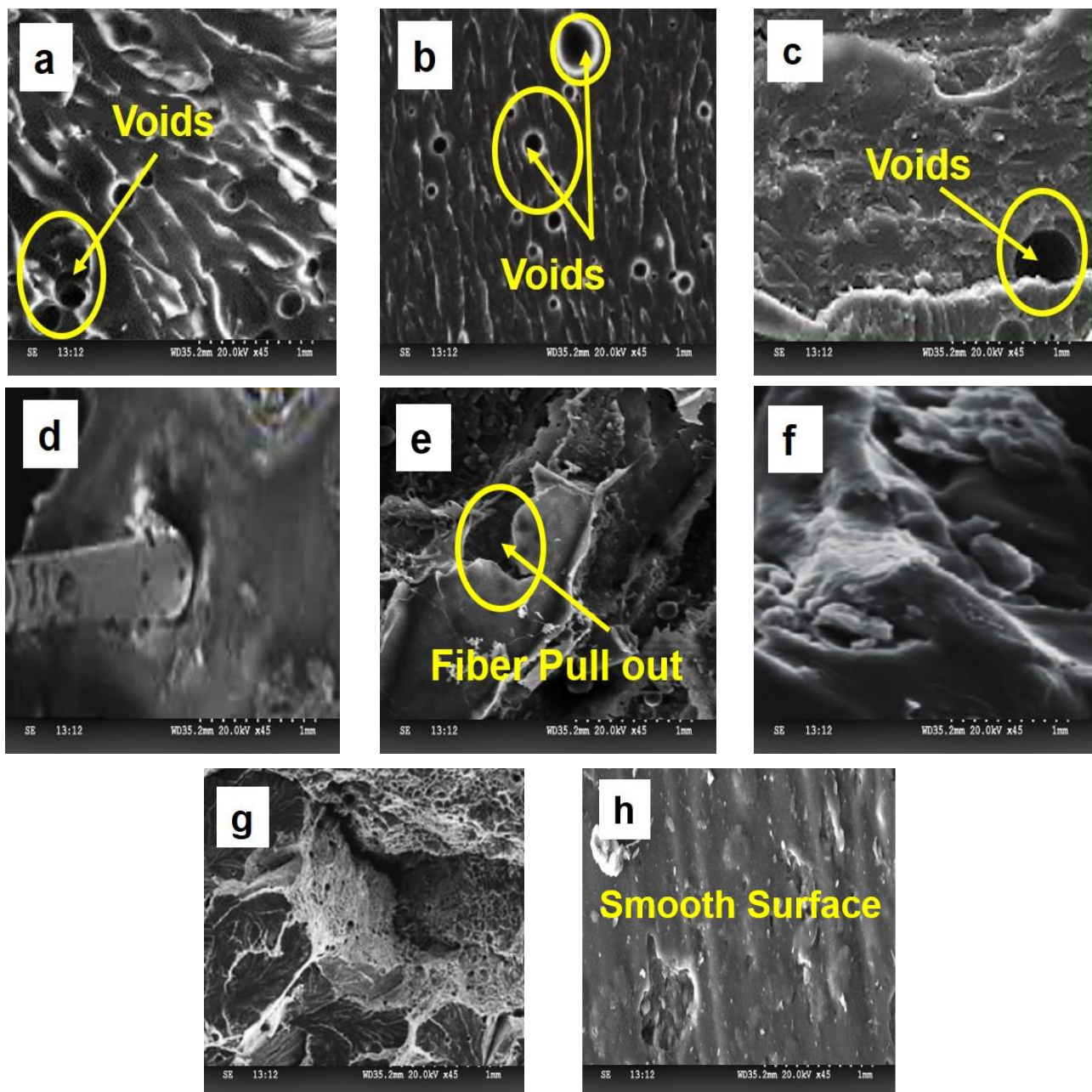

Figure 14. Microstructural Images of (**a**) Plain epoxy; (**b**) 0 wt.% of NaOH Treated; (**c**) 1 wt.% NaOH Treated; (**d**) 3 wt.% of NaOH Treated; (**e**) 5 wt.% of NaOH Treated composites; (**f**) 5 wt.% NaOH Treated Tensile failure; (**g**) 5 wt.% NaOH Treated Flexural failure; (**h**) 5 wt.% NaOH Treated Impact failure.

3.4. Water Absorption Behaviour

Figure 15a–d depict the proportion of water absorbed by sisal- and flax-fibre-reinforced hybrid composites following different concentrations of NaOH treatment (0, 1 wt.%, 3 wt.%, and 5 wt.%). The Indians' attitudes toward water have shifted drastically through time. Fibre reinforcement generally causes polymer composites to retain a lot of moisture. The moisture absorption of flax- and sisal-fibre-reinforced composite materials with 3 wt.% and 5 wt.% NaOH concentrations was moderate, whereas the moisture content of NaOH-treated flax- and sisal-fibre-reinforced composite materials with 1 wt.% and 0 wt.% concentrations was high. The mechanical-fractured sample study revealed that fibre composites containing

5% NaOH had strong fibre-to-matrix bonding capabilities. As a consequence, excellent water-resistant characteristics were developed. Due to good bonding, the polymer matrix is tightly wrapped around the fibre, preventing water molecules from contacting the exterior [45]. Liquid fragments may effortlessly enter the fibre surface in the 0-wt.% and 1 wt.% fibre-reinforced composites due to the weak interaction between the matrix and the fibre. As a consequence, the water absorption of the material increased. The 0-wt.%, 1 wt.%, 3 & 5 wt.% flax- and sisal-fibre-reinforced composites reached saturation point after 60 h of incubation. As can be observed, all nanomaterials display a normal polymeric water uptake response that follows Fick's baseline. In general, including nanofillers reduces the water absorption of altered hybrids compared to ordinary epoxy. The nanofiller's exceptional resistance characteristics cause this phenomenon. Including nanofillers with a high surface area can provide a difficult route for hydrogen atoms to infiltrate into the nanocomposite. The maximal water absorption of aluminium oxide reinforced polymer nanocomposites diminishes steadily as the filler concentration increases [41]. Compared to plain epoxy, the maximum moisture uptake of aluminium-loaded epoxy nanomaterials is reduced by 12.1, 19.4, and 22.4%, respectively, with the inclusion of 2, 4, and 6 wt.% aluminium oxide. Similarly, adding 2, 4, and 6 wt.% aluminium oxide reduces water retention by 9.14, 10.21, and 16.54%, respectively. Surprisingly, the resistance characteristics of nanomaterials loaded with aluminium oxide outperform those of other unfilled biocomposites.
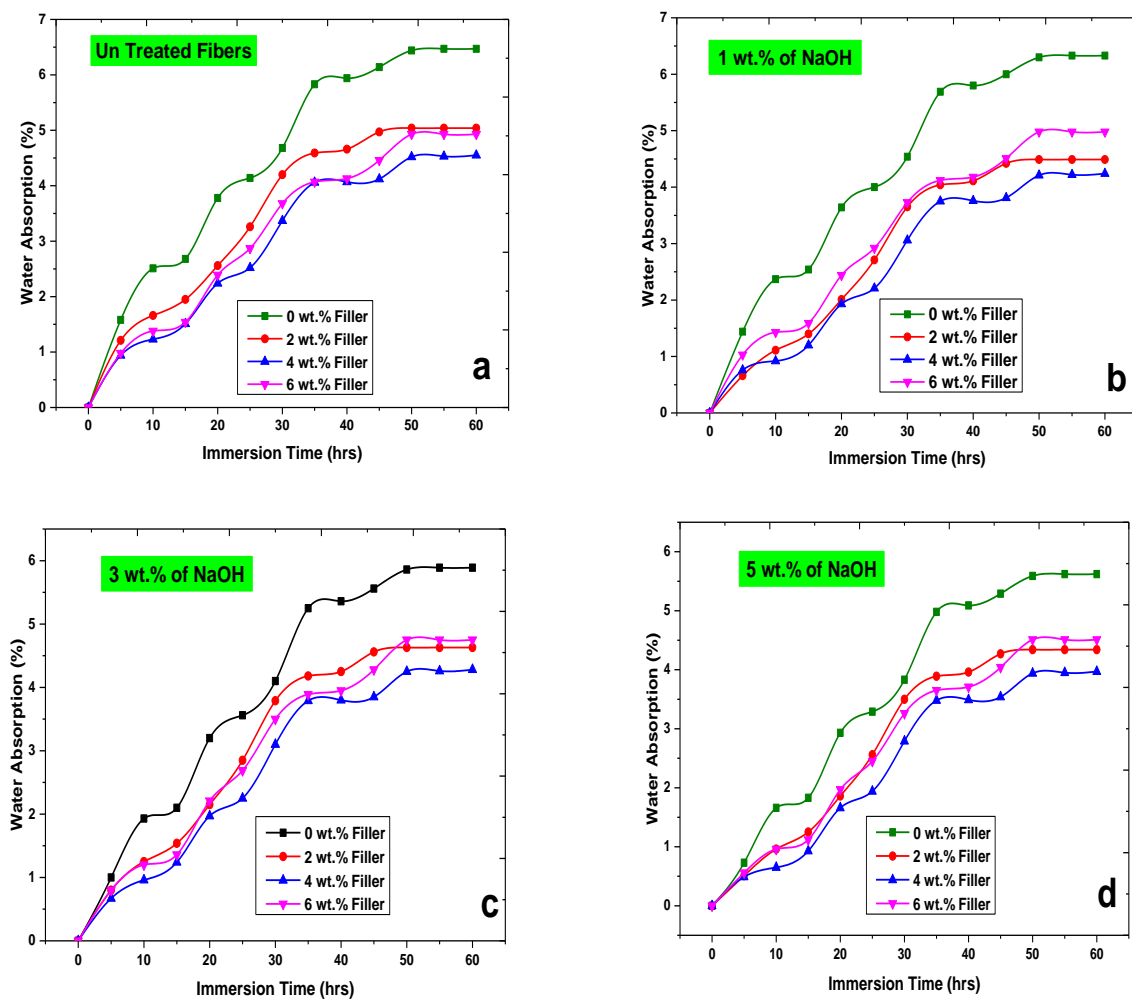

Figure 15. Moisture Absorption Behaviours of (**a**) Untreated; (**b**) 1 wt.% of NaOH; (**c**) 3 wt.% of NaOH; (**d**) 5 wt.% NaOH treated sisal/flax/Nano Al_2O_3/Epoxy based hybrid composites.

4. Conclusions

This is a new attempt to make a hybrid composite that includes biosynthesized nanoparticles with different concentrations and fibre content with NaOH processing. The flax/sisal-fibre-reinforced epoxy-based hybrid nano Al_2O_3 NPs particle accompaniments of biocomposites were successfully fabricated through the compression moulding method and the following observations were made.

- The XRD characteristic of Al_2O_3-NPs exhibits three diffraction patterns (115, 119, and 215). Powder X software was used to identify these peaks, which were discovered to correlate with the composition of Al_2O_3 NPs. TEM images were also used to confirm the spherical structure of Al_2O_3 NPs.
- According to the HPLC results, the leaf's overall concentrations of flavonoids (gallocatechin, carnosic acid, and camellia) are determined to be 0.250 mg/g, 0.264 mg/g, and 0.552 mg/g, respectively. The catechin concentration is higher than the phenolic and caffeic acid levels, which could have resulted in a faster rate of reduction. This contributes to the formation of Al_2O_3 NPs.
- Among many of the varying configurations, 4 wt.% nano Al_2O_3 NPs, 10 wt.% flax and sisal fibres, as well as 4 h of NaOH with a 5 wt.% concentration, produce the maximum mechanical properties (59.94 MPa tension, 149.52 MPa bending, and 37.9 KJ/m^2 impact resistance).
- In comparison to 0, 2, 4 as well as 6 wt.% nano Al_2O_3 NPs, 4 wt.% nano Al_2O_3 NPs incorporation has the maximum mechanical properties owing to the Al_2O_3 particles being well combined in the epoxy matrix and exhibiting good interfacial adhesion strength.
- Compared to plain epoxy, the maximum moisture uptake of aluminium-loaded epoxy nanomaterials is reduced by 12.1, 19.4, and 22.4%, respectively, with the inclusion of 2, 4, and 6 wt.% aluminium oxide. This is because the resistance characteristics of natural composites loaded with aluminium oxide outperform those of other unfilled biocomposites.

References

1. Ramesh, M.; Palanikumar, K.; Reddy, K.H. Mechanical Property Evaluation of Sisal-Jute-Glass Fiber Reinforced Polyester Composites. *Compos. B Eng.* **2013**, *48*, 1–9. [CrossRef]
2. Yasir, M.; Al, A.; Ullah, Z.; Ahmed, W.; Arshad, H.; Ali, A. Results in Engineering Natural Fiber Reinforced Composites: Sustainable Materials for Emerging Applications. *Results Eng.* **2021**, *11*, 100263. [CrossRef]

3. Velmurugan, G.; Natrayan, L.; Rao, Y.S.; Gaur, P.; Sekar, S.; Chebolu, R.; Patil, P.P.; Paramasivam, P. Influence of Epoxy / Nanosilica on Mechanical Performance of Hemp / Kevlar Fiber Reinforced Hybrid Composite with an Ultrasonic Frequency. *Adsorpt. Sci. Technol.* **2022**, *2022*, 7233255. [CrossRef]

4. Saba, N.; Paridah, M.T.; Abdan, K.; Ibrahim, N.A. Effect of Oil Palm Nano Filler on Mechanical and Morphological Properties of Kenaf Reinforced Epoxy Composites. *Constr. Build. Mater.* **2016**, *123*, 15–26. [CrossRef]

5. Li, Y.; Mai, Y.; Ye, L. Sisal Fibre and Its Composites: A Review of Recent Developments IM PA US AS DO ME US EX ON AS. *Compos. Sci. Technol.* **2000**, *60*, 2037–2055. [CrossRef]

6. Sathish, T.; Natrayan, L.; Christydass, S.P.J.; Sivananthan, S.; Kamalakannan, R.; Vijayan, V.; Paramasivam, P. Experimental Investigation on Tribological Behaviour of AA6066: HSS-Cu Hybrid Composite in Dry Sliding Condition. *Adv. Mater. Sci. Eng.* **2022**, *2022*, 9349847. [CrossRef]

7. Yan, L.; Chouw, N.; Jayaraman, K. Flax Fibre and Its Composites—A Review. *Compos. B Eng.* **2014**, *56*, 296–317. [CrossRef]

8. Charlet, K.; Baley, C.; Morvan, C.; Jernot, J.P.; Gomina, M.; Bréard, J. Characteristics of Hermès Flax Fibres as a Function of Their Location in the Stem and Properties of the Derived Unidirectional Composites. *Compos. A Appl. Sci. Manuf.* **2007**, *38*, 1912–1921. [CrossRef]

9. Sabarinathan, P.; Annamalai, V.E.; Vishal, K.; Nitin, M.S.; Natrayan, L.; Veeeman, D.; Mammo, W.D. Experimental study on removal of phenol formaldehyde resin coating from the abrasive disc and preparation of abrasive disc for polishing application. *Adv. Mater. Sci. Eng.* **2022**, *2022*, 6123160. [CrossRef]

10. Evtimova, M.; Vlahova, M.; Atanassov, A. Flax Improvement by Biotechnology Means. *J. Nat. Fibers* **2005**, *2*, 17–34. [CrossRef]

11. Neto, J.S.S.; Lima, R.A.A.; Cavalcanti, D.K.K.; Souza, J.P.B.; Aguiar, R.A.A.; Banea, M.D. Effect of Chemical Treatment on the Thermal Properties of Hybrid Natural Fi Ber-Reinforced Composites. *J. Appl. Polym. Sci.* **2018**, *136*, 47154. [CrossRef]

12. de Lima, R.A.A.; Cavalcanti, D.K.; Banea, M.D.; Neto, J.S.S.; Meneses, H. Effect of Surface Treatments on Interfacial Properties of Natural Intralaminar Hybrid Composites. *Polym. Compos.* **2019**, *41*, 314–325. [CrossRef]

13. Safri, S.N.A.; Sultan, M.T.H.; Jawaid, M.; Jayakrishna, K. Impact behaviour of hybrid composites for structural applications: A review. *Compos. B Eng.* **2017**, *133*, 112–121. [CrossRef]

14. Cavalcanti, D.K.K.; Banea, M.D.; Neto, J.S.S.; Lima, R.A.A.; Silva, L.F.M.; Carbas, R.J.C. Mechanical characterization of intralaminar natural fibre-reinforced hybrid composites. *Compos. B Eng.* **2019**, *175*, 107149. [CrossRef]

15. Velmurugan, G.; Shankar, V.S.; Rahiman, M.K.; Prathiba, R.; Dhilipnithish, L.R.; Khan, F.A. Effectiveness of Silica Addition on the Mechanical Properties of Jute / Polyester Based Natural Composite. *Mater. Today Proc.* **2022**. [CrossRef]

16. Meikandan, M.; Karthick, M.; Natrayan, L.; Patil, P.P.; Sekar, S.; Rao, Y.S.; Bayu, M.B. Experimental Investigation on Tribological Behaviour of Various Processes of Anodized Coated Piston for Engine Application. *J. Nanomater.* **2022**, *2022*, 7983390. [CrossRef]

17. Li, Y.; Guo, X.; Yang, J.; Li, M. Preparation of Nano-SiO 2 / Carbon Fiber-Reinforced Concrete and Its Influence on the Performance of Oil Well Cement. *Int. J. Polym. Sci.* **2019**, *2019*, 1–9.

18. Paranthaman, V.; Sundaram, K.S.; Natrayan, L. Influence of SiC particles on mechanical and microstructural properties of modified interlock friction stir weld lap joint for automotive grade aluminium alloy. *Silicon* **2022**, *14*, 1617–1627. [CrossRef]

19. Alharthi, N.S.; Aldakheel, F.M.; Binshaya, A.S. Inhibition of Glycogen Synthase Kinase and the Neuroprotective Function of Conjugated ZnO-Osthol Nanoparticles in Alzheimer's Disease. *Bioinorg. Chem. Appl.* **2022**, *2022*, 1401995. [CrossRef]

20. Wang, S.; Hu, Z.; Lu, S. Research on Microseismic Source Location Method Based on Waveform Characteristics Monitored by Nanomaterial Sensor under the Background of Metal Oxide Polluted Environment. *Bioinorg. Chem. Appl.* **2022**, *2022*, 5479007. [CrossRef]

21. Li, C.; Xiang, Y.; Wang, Y.; Li, P. Study on Nano Drug Particles in the Diagnosis and Treatment of Alzheimer's Disease in the Elderly. *Bioinorg. Chem. Appl.* **2022**, *2022*, 3335581. [CrossRef] [PubMed]

22. Hlapisi, N.; Motaung, T.E.; Linganiso, L.Z.; Oluwafemi, O.S.; Songca, S.P. Encapsulation of Gold Nanorods with Porphyrins for the Potential Treatment of Cancer and Bacterial Diseases: A Critical Review. *Bioinorg. Chem. Appl.* **2019**, *2019*, 7147128. [CrossRef] [PubMed]

23. Nasrollahzadeh, M.; Issaabadi, Z.; Sajadi, S.M. Green Synthesis of the Ag / Al 2 O 3 Nanoparticles Using Bryonia Alba Leaf Extract and Their Catalytic Application for the Degradation of Organic Pollutants. *J. Mater. Sci. Mater. Electron.* **2019**, *30*, 3847–3859. [CrossRef]

24. Gao, H.; Fan, A. Green synthesis of 1,5-dideoxy-1,5-imino-ribitol and 1,5-dideoxy-1,5-imino-dl-arabinitol from natural d-sugars over Au/Al_2O_3 and SO_4^{2-}/Al_2O_3 catalysts. *Sci. Rep.* **2021**, *11*, 16928. [CrossRef]

25. Matheswaran, M.; Arjunan, T.; Muthusamy, S.; Natrayan, L.; Panchal, H.; Subramaniam, S.; Khedkar, N.; El-Shafay, A.S.; Sonawane, C. A case study on thermo-hydraulic performance of jet plate solar air heater using response surface methodology. *Case Stud. Therm. Eng.* **2022**, *34*, 101983. [CrossRef]

26. Sánchez-Navarro, M.; Ruiz-torres, C.A.; Niño-Martinez, N.; Sánchez-Sánchez, R.; Martínez-Castañón, G.A.; DeAlba-Montero, I.; Ruiz, F. Cytotoxic and Bactericidal Effect of Silver Nanoparticles Obtained by Green Synthesis Method Using Annona Muricata Aqueous Extract and Functionalized with 5-Fluorouracil. *Bioinorg. Chem. Appl.* **2018**, *2018*, 6506381. [CrossRef]

27. Uluçam, G.; Turkyilmaz, M. Synthesis, Structural Analysis, and Biological Activities of Some Imidazolium Salts. *Bioinorg. Chem. Appl.* **2018**, *2018*, 1439810. [CrossRef]

28. Wali, L.A.; Hasan, K.; Alwan, A. An Investigation of Efficient Detection of Ultra-Low Concentration of Penicillins in Milk Using AuNPs / PSi Hybrid Structure. *Plasmonics* **2020**, *15*, 985–993. [CrossRef]

29. Khan, R.A.; Aurel, T.; Ali, F.; Koo, B.H. Anticancer and Antimicrobial Properties of Inorganic Compounds / Nanomaterials. *Bioinorg. Chem. Appl.* **2019**, *2019*, 6019632. [CrossRef]

30. Wali, L.A.; Alwan, A.M.; Dheyab, A.B.; Hashim, D.A. Excellent fabrication of Pd-Ag NPs/PSi photocatalyst based on bimetallic nanoparticles for improving methylene blue photocatalytic degradation. *Optik* **2019**, *179*, 708–717. [CrossRef]

31. Zhang, W. Nanoscale Iron Particles for Environmental Remediation: An Overview. *J. Nanopart. Res.* **2003**, *5*, 323–332. [CrossRef]

32. Nishitani, E.; Sagesaka, Y.M. Simultaneous Determination of Catechins, Caffeine and Other Phenolic Compounds in Tea Using New HPLC Method. *J. Food Compos. Anal.* **2004**, *17*, 675–685. [CrossRef]

33. Wang, T.; Lin, J.; Chen, Z.; Megharaj, M.; Naidu, R. Green Synthesized Iron Nanoparticles by Green Tea and Eucalyptus Leaves Extracts Used for Removal of Nitrate in Aqueous Solution. *J. Clean. Prod.* **2014**, *83*, 413–419. [CrossRef]

34. Jabbar, A.A.; Alwan, A.M.; Zayer, M.Q.; Bohan, A.J. Efficient Single Cell Monitoring of Pathogenic Bacteria Using Bimetallic Nanostructures Embedded in Gradient Porous Silicon. *Mater. Chem. Phys.* **2020**, *241*, 122359. [CrossRef]

35. Bandeira, M.; Possan, A.L.; Pavin, S.S.; Raota, C.S.; Vebber, M.C.; Giovanela, M.; Roesch-ely, M.; Devine, D.M. Nano-Structures & Nano-Objects Mechanism of Formation, Characterization and Cytotoxicity of Green Synthesized Zinc Oxide Nanoparticles Obtained from Ilex Paraguariensis Leaves Extract. *Nano-Struct. Nano-Objects* **2020**, *24*, 100532. [CrossRef]

36. Purkait, P.; Bhattacharyya, A.; Roy, S.; Maitra, S.; Das, G.C.; Chaudhuri, M.G. Green Synthesis of TiO2 Nanoparticle: Its Characterization and Potential Application in Zoxamide Photodegradation. *J. Water Environ. Nanotechnol.* **2020**, *5*, 191–203. [CrossRef]

37. Rangappa, S.M.; Parameswaranpillai, J.; Siengchin, S. Bioepoxy Based Hybrid Composites from Nano—Fillers of Chicken Feather and Lignocellulose Ceiba Pentandra. *Sci. Rep.* **2022**, *12*, 1–18. [CrossRef]

38. Bitire, S.; Jen, T.-C. South African Journal of Chemical Engineering The Role of a Novel Green Synthesized Nanoparticles Added Parsley Biodiesel Blend on the Performance-Emission Characteristics of a Diesel Engine. *S. Afr. J. Chem. Eng.* **2022**, *41*, 161–175. [CrossRef]

39. Okonkwo, E.C.; Abid, M.; Ratlamwala, T.A.H.; Abbasoglu, S.; Dagbasi, M. Optimal Analysis of Entropy Generation and Heat Transfer in Parabolic Trough Collector Using Green-Synthesized TiO2/Water Nanofluids. *J. Sol. Energy Eng.* **2018**, *141*, 031011. [CrossRef]

40. Velmurugan, G.; Babu, K. Statistical Analysis of Mechanical Properties of Wood Dust Filled Jute Fiber Based Hybrid Composites under Cryogenic Atmosphere Using Grey-Taguchi Method. *Mater. Res. Express* **2020**, *7*, 065310. [CrossRef]

41. Balasubramani, V. Effect of Surface Treatment on Natural Fibers Composite Effect of Surface Treatment on Natural Fibers Composite. *IOP Conf. Ser. Mater. Sci. Eng.* **2018**, *376*, 012053. [CrossRef]

42. Koopi, H.; Buazar, F. A novel one-pot biosynthesis of pure alpha aluminum oxide nanoparticles using the macroalgae *Sargassum ilicifolium*: A green marine approach. *Ceram. Int.* **2018**, *44*, 8940–8945. [CrossRef]

43. Manikandan, V.; Jayanthi, P.; Priyadharsan, A.; Vijayaprathap, E.; Anbarasan, P.M.; Velmurugan, P. Green synthesis of pH-responsive Al2O3 nanoparticles: Application to rapid removal of nitrate ions with enhanced antibacterial activity. *J. Photochem. Photobiol. A Chem.* **2019**, *371*, 205–215. [CrossRef]

44. Subramanian, B.; Lakshmaiya, N.; Ramasamy, D.; Devarajan, Y. Detailed analysis on engine operating in dual fuel mode with different energy fractions of sustainable HHO gas. *Environ. Prog. Sustain. Energy* **2022**, *41*, e13850. [CrossRef]

45. Rasheed, T.; Bilal, M.; Iqbal, H.M.N.; Li, C. Green Biosynthesis of Silver Nanoparticles Using Leaves Extract of Artemisia Vulgaris and Their Potential Biomedical Applications. *Colloids Surf. B Biointerfaces* **2017**, *158*, 408–415. [CrossRef]